

MDM:Visual Explanations for Neural Networks via Multiple Dynamic Mask

Yitao Peng, Longzhen Yang, Yihang Liu, Lianghua He*

College of Electronic and Information Engineering Tongji University

4800 Cao'an Highway, Shanghai, China 201804

{pty, yanglongzhen, 2111131, helianghua}@tongji.edu.cn

Abstract

The Class Activation Maps(CAM) lookup of a neural network can tell us what regions the neural network is focusing on when making a decision, which gives us a basis for interpretability when the neural network makes a classification decision. In the past, the CAM search method used the result of the operation of a specific internal module of the network, and deduced the saliency map activated in the original picture through a specific algorithm method. It does not have the interpretability of the inference process, has specific constraints on the structure of the neural network, and has poor lookup performance. We propose an algorithm Multiple Dynamic Mask (MDM), which is a general saliency graph query method with interpretability of inference process. The algorithm is based on an assumption: when a picture is input into a trained neural network, only the activation features related to classification will affect the classification results of the neural network, and the features unrelated to classification will hardly affect the classification results of the network. MDM: A learning-based end-to-end algorithm for finding regions of interest for neural network classification. It has the following advantages: 1. It has the interpretability of the reasoning process, and the reasoning process conforms to human cognition. 2. It is universal, it can be used for any neural network and does not depend on the internal structure of the neural network. 3. The search performance is better. The algorithm is based on learning and has the ability to adapt to different data and networks. The performance is better than the method proposed in the previous paper. For the MDM saliency map search algorithm, we experimentally compared ResNet and DenseNet as the trained neural network. The recent advanced saliency map search method and the results of MDM on the performance indicators of each search effect item, the performance of MDM has reached the state of the art. We applied the MDM method to the interpretable neural network ProtoPNet and XProtoNet, which improved the model's interpretability prototype search performance. And we visualize the effect of convolutional neural architecture and Transformer architecture in saliency map search, illustrating the interpretability and generality of MDM.

1. Introduction

Neural networks [16, 17, 18, 19, 20, 23, 24] have achieved remarkable success in the field of image classification, and the explanation of neural network decisions is starting to gain attention.

Since the neural network is a black-box model, humans cannot understand the decision-making of the neural network, and it is difficult to build trust in such models, so that the neural network is difficult to apply to some important fields, such as: pathological diagnosis, unmanned driving. In medical field, whether the diagnosis results of neural networks are credible is a major issue related to life. Although many models [25, 26] can achieve good results in the field of medical diagnosis and even surpass human doctors, but [21] without a good explanation of the model's decisions, neither doctors nor patients can trust the model, which is why neural networks with better classification performance still cannot be used in the clinical field.

Based on the above requirements for explaining neural networks, various methods [1, 2, 3, 5, 6, 7, 8, 9] have been proposed for explaining models. [21] thinks that the methods of explaining neural network models are divided into: explaining the reasoning process of the neural network and explaining the information of the neural network module. The explanation of the inference process is to make the inference process of the model conform to human cognition. By setting the model to conform to some accepted reasoning process, the model's decisions can be

understood and trusted. Interpretation of neural network module information, by studying the gradients of some modules of the neural network and the activation of some internal hidden layers to determine which areas of the image are promoting the neural network to make decisions.

The above neural network interpretation methods have their own limitations. There are [1, 2, 3, 5, 6] methods for the interpretation of neural network module information, which require specific restrictions on the internal structure of the neural network. For example, CAM needs to capture the global average pooling layer information at the end of the neural network. . This approach is difficult to transfer to recent state-of-the-art neural network models, such as those of the Transformer architecture [19, 20]. This type of method is less general.

The neural network ProtoPNet [12], XProtoNet [13] and other models of the classification of the interpretability of the reasoning process need to be set to a specific interpretable architecture, resulting in poor network performance. And the above paper's search method for the interpretable prototype prototype is to use the feature map upsampling to the original image size to represent the activation, which is not only not interpretable, but also has poor performance in finding prototypes that explain the classification of the model.

The MDM proposed in this paper is a learning-based, general, and interpretable neural network decision region search method, which can find the decision activation region of the neural network to explain the region that the neural network pays attention to when making classification decisions. The structure of MDM is shown in Figure 1. First, its interpretability is based on an assumption: the decision of the neural network only depends on the information of the classification target, and the information of the non-classification target hardly affects the decision of the neural network. Through this assumption, the classification decision basis of the neural network is obtained indirectly.

In almost most neural network classification tasks, its decision process takes the classification target as foreground information, and makes classification by finding the foreground information in the graph as the basis for decision-making, even if the background information irrelevant to classification is erased or modified It should also barely affect the neural network to make the classification. Because the neural network makes the correct classification based on the foreground information, which is an essential content for making correct decisions and is invariant. The background belongs to auxiliary information or redundant information can be changed arbitrarily. The neural network makes the correct classification only when it sees the basis for classification, and this process is in line with the fact of human cognition.

Based on the above assumption, MDM explains the reasoning process of the neural network by retaining the decision-making information that is beneficial to the classification of the image in the neural network and removing the redundant information that is not conducive to the classification of the neural network. The reasoning process of the MDM is the same as the human decision-making process and can explain any neural network's decision to classify image data.

Because MDM regards the neural network structure as a black box and does not use the structural information inside the network, it can be applied to any structure of the neural network and has good generality.

MDM is a learning-based method, which has more adaptability to different input data and different network structures, so that it has better search performance for explaining the classification basis of neural networks. In our multiple experiments comparing the most advanced models in recent years, MDM has achieved state-of-the-art in all indicators.

The main contributions of this paper can be summarized as follows:

- We propose a general, interpretable, and better-performing method for finding basis for classification decisions in neural networks. And we give a mathematical proof of the feasibility of the MDM algorithm under certain conditions.

- On the traditional convolutional neural network, the performance of other mainstream neural network interpretability search methods are compared, and the search performance of the MDM method in the neural network decision area is verified to achieve state-of-the-art.

- The MDM method is applied to the interpretable neural networks ProtoPNet and XProtoNet of traditional image datasets and pathological image datasets, which greatly improves

the performance of the above neural networks in classifying traditional images and medical images.

- The MDM is applied to the current state-of-the-art convolutional neural networks ResNet, VGG, DenseNet and the neural networks VIT and Swin-Transformer of the Transformer architecture, and the decision-making basis for the classification and prediction of the neural network is visualized. Validating that the MDM method is also applicable to these advanced neural networks with non-specific convolutional neural network architectures, further illustrates the generality of the method.

2. Related Work

The interpretation of neural network classification can be divided into using neural network module information to explain neural network predictions, and using interpretable reasoning processes to explain neural network predictions.

The Global Average Pooling (GAP) proposed by Lin [4], the global average pooling integrates the information of the feature to the whole space. In 2015, Zhou [2] first proposed to use GAP global average pooling to obtain feature vectors, and then fully connect with the output layer to obtain Class Activation Maps (CAM). Since the CAM method requires that the neural network must have an average pooling layer, it can only be applied to a network with a specific structure where the feature map extraction operation of the last layer is a GAP operation. R. Selvaraju [1] proposed Grad-CAM, which only needs to use the gradient. Obtaining activation maps makes the method of obtaining CAM more universal. In 2017, Chattpadhyay [3] proposed an improved version of Grad-CAM++, which believes that each element on the gradient map contributes differently, so an additional weight is added to weight the elements on the gradient map to optimize the results of Grad-CAM , which makes the CAM localization more accurate and more suitable for the situation where there is more than one object of the target category in the image. Shrikumar [8] proposed Deep Learning Important FeaTures (DeepLIFT) to decompose the neural network's output prediction for a specific input by back-propagating the contribution of all neurons in the network to each feature of the input. Sundararajan [9] proposed Integrated Gradients (IG) to find out the input features for the prediction attribution of deep networks by making several calls to the gradient of the standard operator. In 2019, Wang [5] proposed a gradient-free approach, Score-CAM, which defined the concept of Increase of Confidence (ICI). To a certain extent, the problems of neural network gradient noise, saturation and easy to find false confidence samples are solved. In 2020, Desai [6] proposed Ablation-CAM, which traversely juxtaposes the feature maps of each layer to 0 and then performs network forward calculation to obtain the target category score. The relative size of this value and the original score is used as the feature map fusion weight. Control variables to remove various components, etc. to explore the strength of each factor's contribution to the overall model, and find the most important factor affecting performance.

The above methods are to extract certain module information inside the neural network to study the activation of the neural network for decision-making. Its derivation is not easy for humans to understand, and it is not convenient to migrate from one model to another new model. For example, neural networks with Transformer architecture with self-attention mechanism, because their specific structure is different from traditional convolutional neural network architecture, the above methods are not easy to transfer to the network of this architecture. Therefore, the generality of the above method is poor.

Interpretability based on inference process: Petsiuk [7] proposed a neural network interpretability analysis method RISE for black-box models, and provided a method for evaluating the interpretability performance of model activation maps, insertion and deletion . The length and width of all masks used by RISE are the same, so that the area that each receiving field can accept is the same, resulting in redundant and not necessarily complete extracted information. And it sets each element in the initial mask to the value limit {0, 1}, so that the fitting space of the model is relatively small, and the mask expression ability is insufficient, resulting in poor model performance. Chen [12] proposed ProtoPNet, which is an interpretable neural network. The

network structure it designs conforms to the human reasoning process, inferring the category of the input data by finding whether the input picture has a similar prototype for a certain category. It defines a prototype as a eigenvector with a length and a width of 1. Kim [13] proposed an improved network XProtoNet to set the prototype as a feature vector with variable activation location and size, and applied it to the interpretable classification of X-ray images of chest diseases. SINGH [14, 15] proposed improved networks NP-ProtoPNet and Gen-ProtoPNet based on ProtoPNet, which further generalized the size of feature vector blocks representing prototypes, and applied the method to COVID-19 detection.

The network with the above ProtoPNet structure upsamples the prototype activation feature map into an activation map of the original image size, and uses its larger activation area as the neural network classification basis. First, this method of extracting prototypes is not interpretable. Because, the original image is input into the feature map obtained by the complex neural network, and the numerical value has no theoretical basis to support that the corresponding position of the larger numerical value region in the feature map is the corresponding position of the corresponding activation region in the original image. Second, this direct upsampling method has poor lookup performance. The MDM proposed in this paper can be applied to these networks. As a network prototype search method, it not only greatly improves the prototype search performance, but also the search process is interpretable.

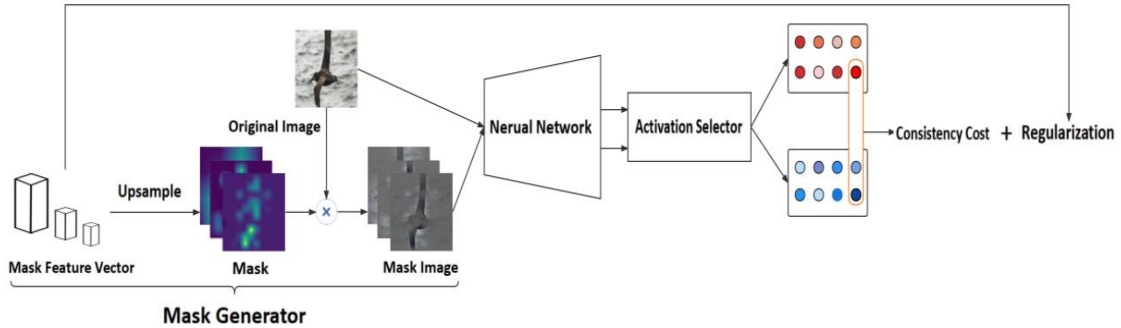


Figure 1. Overall architecture of Multiple Dynamic Mask.Train mask vector through above architecture.

3.Method

Multiple Dynamic Mask

We introduce the overall architecture and objective function in Section 3.1, and describe the training process in Section 3.2. We explain in Section 3.3 how to generate mask via multiple feature mask vectors. And the activation map is generated in Section 3.3. In Section 3.4, we describe the mathematical feasibility of the algorithm.

3.1. Architecture and Objective Function

MDM consists of mask generator, neural network, activation selector. By maximizing the mask while preserving the decision information favorable for classification. The objective function of mask training and mask generation represented by it is:

Train function:

$$\min_{d_i} \|f_p(X) - f_p(g(d_i)X)\|^2 + \lambda_i \frac{1}{|a_i b_i|} \sum_{u=1}^{a_i} \sum_{v=1}^{b_i} |d_{iuv}| \quad (1)$$

Generate function:

$$M^h = \text{Normalize}(\{ \sum_{i=1}^N g(d_i) \geq \gamma \} \sum_{i=1}^N g(d_i)) \quad (2)$$

Mask Generator. Set the appropriate N mask feature vectors $D \{d_i\}_{i=1}^N$ to be trained for the dataset, $d_i \in R^{a_i \times b_i \times 1}$, where each value in d_i is set as a fixed value. Satisfy any $i, j \in \{1, \dots, N\}$, $a_i \neq a_j$ or $b_i \neq b_j$. Select the mask feature vector transformation function $g(\cdot)$ to generate mask $M_i = g(d_i) \in R^{H \times W \times 1}$, where $g(\cdot)$ contains the normalization operation, so each element in M_i value $\in [0, 1]$. $M_i X$ and X are inputs for calculating the activation consistency of neural network f , and d_i and mask $M_i = g(d_i)$ are obtained by minimizing the objective function (1).

As shown in Figure 2: the smaller the size of d_i , the larger the receptive field corresponding to each element point in d_i , the more semantic information it contains, and the more accurate f makes decisions. (1) The training mask performance is better, but the disadvantage is that the mask The granularity of the activation area division is too large, the spatial information is less, and the spatial feature division is not fine. On the contrary, when the size of d_i is larger, the corresponding receptive field is smaller, and the mask division space area is more refined, but the semantic information of each receptive field is less, the activation accuracy of the calculated activation area is lower, and the mask performance is poor.

We need to consider both the accuracy of semantic information and the accuracy of spatial information. Therefore, by stacking d_i masks of various sizes, the generated masks can better balance the above two accuracy and obtain better results. robustness. When the receptive field corresponding to a single element point of d_i is too small, the classification performance of the neural network f is not good, and an adversarial effect will occur [7]. Therefore, we set a lower threshold to remove the activation areas smaller than the threshold, and remove these redundant or erroneous ones. Activation message culling. The mask calculation formula we provide is (2).

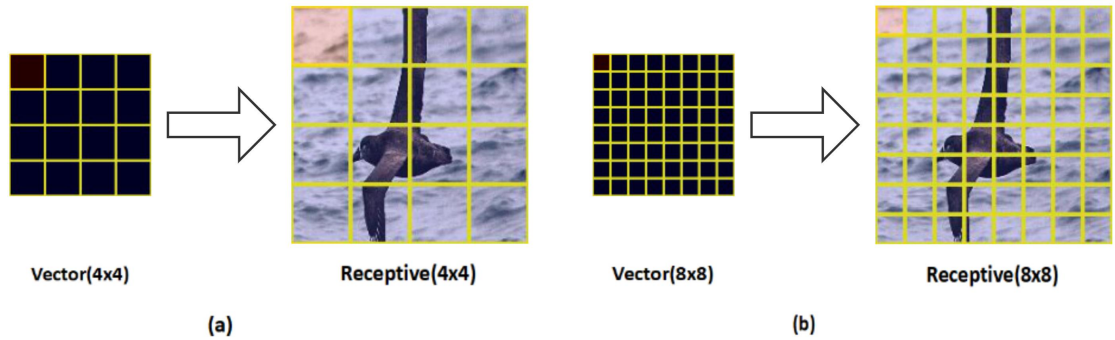


Figure 2. After d_i of different sizes is upsampled to the original image size, the receptive field corresponding to each pixel point. (a) indicates that d_i is a 4×4 size mask feature vector, and each pixel in d_i corresponds to a 56×56 size area(red area) in the original image after upsampling. In (b) d_i is a mask feature vector of size 8×8 , and each pixel in d_i corresponds to a 28×28 area(red area) in the original image after upsampling. The larger the d_i size is, the smaller the receptive field area of the original image corresponding to each pixel is.

Neural Network.Since this process does not rely on the information of the internal structure of the neural network, it only pays attention to the input and output of the neural network. Therefore, MDM can be used on neural networks of any structure. Just put the trained neural network into this module, fix the parameters of the neural network unchanged, and use the output of the mask generator as the input. The activation selector selects some nodes of the neural network as activation regions.

Activation selector.The activation selector module selects the specific activation area of the neural network, so that the original image and the mask image are activated consistently in the activation area to train the mask vector. The specific activation area needs a corresponding setting for the classification task and network structure. General classification neural network such as: ResNet, VIT, their output is to get the *logits* of each class after going through the classification layer, and classify according to the size of the *logits*. We perform a filter on the *logits* output by the neural network, keeping the value and position of the *logits* of the class corresponding to the classification decision we want to know. If we want to explain the neural network's choice of the class corresponding to the largest *logits*, then keep the value and position of the *logits* of that largest class as the activation choice. If we want to examine the choice of some other class, set the value and position of the *logits* of that class as the activation choice. For example: *logits*=[0.1,0.6,0.3] output by a network, the three positions represent the categories cat, dog, horse respectively, and the network prediction result is dog, then record position 1 and

activation value 0.6 as the neural network is classified as Activation of the dog. For ProtoPNet [12] and XProtoNet [13], their corresponding prototype tensors are selected as activation, respectively.

3.2. Training process

Note: The original image data of Input is (X, Y) . $X \in R^{H \times W \times C}$ is the input image and Y is the classification label. The neural network for the classification task is denoted as f , and t represents the activation position selected by the activation selector.

Mask Generator generates N mask feature vectors $D\{d_i\}_{i=1}^N$, for each mask $M_i = g(d_i)$. The activation of the original image X and the mask image $M_i X$ at the position t after inputting f are expressed as follows (3) and (4), respectively:

$$P_{1,t}^i = f_t(X) \quad (3)$$

$$P_{2,t}^i = f_t(M_i X) \quad (4)$$

Consistency loss, l_1 regularization loss of mask feature vector d_i , total loss as follows(5), (6), (7):

$$Loss_{consistency}^i = \|P_{1,t}^i - P_{2,t}^i\|^2 \quad (5)$$

$$Loss_{l_1}^i = \frac{1}{|a_i b_i|} \|d_i\|_1 = \frac{1}{|a_i b_i|} \sum_{u=1}^{a_i} \sum_{v=1}^{b_i} |d_{iuv}| \quad (6)$$

$$Loss_{total}^i = Loss_{consistency}^i + \lambda_i Loss_{l_1}^i \quad (7)$$

Hyperparameter $\{a_i\}_{i=1}^N$, $\{b_i\}_{i=1}^N$, $\{\lambda_i\}_{i=1}^N$ were selected by 5-fold cross-validation using part of the dataset. Fix all the parameters of the trained neural network f , we use stochastic gradient descent to minimize $Loss_{total}^i$ to train the mask vector d_i , repeat the above operation to obtain N mask feature vectors $\{d_i\}_{i=1}^N$, then the corresponding N masks $\{M_i\}_{i=1}^N$ can be obtained.

As shown in Figure(3), when d_i is training, $Loss_{l_1}^i$ is fixed, and the picture above the *Mask Image* retains a higher mask value in the key decision-making area (the area within the yellow box), resulting in a higher activation consistent with the original image. The image below the *Mask Image* retains a higher mask value in the non-decision area (the area inside the yellow box), and the activation consistency is lower. In order to minimize (7), Mask is therefore constrained to have higher mask values for high activation decision regions and lower mask values for low activation irrelevant regions.

When $Loss_{consistency}^i$ is fixed, minimizing (7) constrains the mask value in the regions of the image that are irrelevant to decisions to be as low as possible.

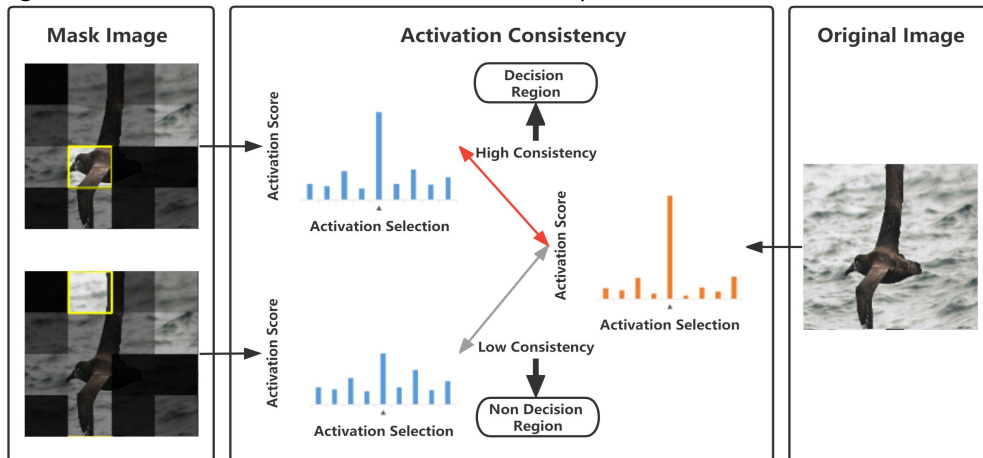


Figure 3. The process of consistent activation and decision-making generated after the two mask images and the original image are input into the neural network. The upper and lower pictures on the left are the pictures generated by the exchange of the mask values of the regions framed by the yellow boxes, and the mask values of the remaining regions remain unchanged. A high activation value indicates that the region that retains a larger mask value may be a decision region, and a low activation value indicates that the region that retains a larger mask value may be a non-decision region.

3.3. Activation map generation

The operation flow is shown in Figure 4. According to the trained $\{d_i\}_{i=1}^N$, the mask $\{M_i\}_{i=1}^N$ and the mask $M_i = g(d_i)$ are generated. Binary mask: $M^b = \{M^F \geq \gamma\}$, γ is the threshold, $\{\cdot\}$ represents the truth function, 1 if the function is true, otherwise 0.

Activation heatmap mask: $M^F = \{\sum_{i=1}^N M_i \geq \gamma\}$, $M^h = \frac{M^F - \mu_F}{\sigma_F}$, where μ_F and σ_F represent the mean and variance of M^h for normalization operations. Original image X , activation heatmap: $\alpha X + \beta M^h$, binary mask image: $M^b X$, the above α , β and γ are hyperparameters.

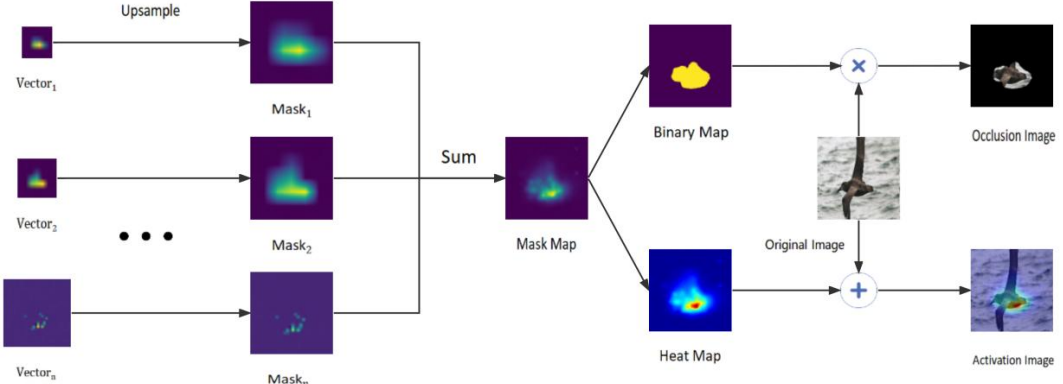


Figure 4. The pipeline of pretrained mask feature vectors to generate binary mask map and activation heatmap for neural network classification decisions.

3.4. Algorithm Feasibility Proof

Proposition P: By calculating the objective function (1), the feature mask vector d_i can be effectively trained, and the up-sampled M_i can mask the classification decision area of the image X , so that the more important decision-making areas are masked lower, vice versa.

The following provides a mathematical proof that the proposition holds under certain assumptions:

Note: Z represents the region in the figure X , and the data of the selected region Z of $f_p(Z)$ is used as input to activate the neural network f at p .

Let: $I(Z) = k f_p(Z)$, where k is a constant greater than zero, $I(Z) \in [0,1]$.

$I(Z)$ represents the amount of information contributed by this region Z to $f_p(Z)$ activation.

Hypothesis 1. When the performance of f is good, the two regions z_1 and z_2 of the mask feature vector under investigation, when the corresponding regions on the original image do not intersect, it is considered that the information I of the contribution of the two regions to activation f is irrelevant. g is the upsampling function.

z_1, z_2 are the two regions of d_i , $i \in \{1, \dots, N\}$,

If $g(z_1) \cap g(z_2) = \emptyset$, then $I(z_1 + z_2) = I(z_1) + I(z_2)$ (8)

Hypothesis 2. The greater the contribution to activation, the greater the contribution to information increment.

z_1, z_2 are the two regions of d_i , $i \in \{1, \dots, N\}$,

$m \in [0,1]$, if $I(z_1) < I(z_2)$, then $0 \leq \frac{\partial I(mz_1)}{\partial m} < \frac{\partial I(mz_2)}{\partial m}$ (9)

(1) It can be abbreviated as the following formula:

$$L(m, z) = [f_p(z) - f_p(mz)]^2 + \lambda(m) \quad (10)$$

z is all areas of d_i , and M is the corresponding mask value on it.

Proposition **Q**: When L in (10) takes the minimum value, the region mask m with higher activation value in d_i is larger, and the region mask m with lower activation value is smaller.

Expressed in mathematical notation:

z_1 and z_2 represent two disjoint regions of d_i .

$\forall z_1, z_2$, if $I(z_1) < I(z_2)$, then $m_1 < m_2$.

Obviously, the original proposition **P** is equivalent to the proposition **Q**. The following proves **Q**. reductio ad absurdum:

If L has obtained the minimum value, and $\exists z_1, z_2$ satisfy: $I(z_1) < I(z_2)$ and $m_1 > m_2$.

Define: $z(d_i)$ means all areas on d_i ,

let: $z_{other} = z(d_i) - z_1 - z_2$, m_{other} represents the mask value of z_{other} .

Obviously: $g(z_1) \cap g(z_2) = \emptyset$, $g(z_1) \cap g(z_{other}) = \emptyset$ and $g(z_2) \cap g(z_{other}) = \emptyset$.

$L(m, z) = L(z_1, m_1, z_2, m_2, z_{other}, m_{other})$

$= [f_p(z_1 + z_2 + z_{other}) - f_p(m_1 z_1 + m_2 z_2 + z_{other})]^2 + \lambda(m_1 + m_2 + m_{other})$

Let: $L'(m, z) = L(z_1, m_2, z_2, m_1, z_{other}, m_{other})$

$S \triangleq 2f_p(z_1 + z_2 + z_{other}) - f_p(m_1 z_1 + m_2 z_2 + z_{other}) - f_p(m_2 z_1 + m_1 z_2 + z_{other}) > 0$

$L'(m, z) - L(m, z) = L(z_1, m_2, z_2, m_1, z_{other}, m_{other}) - L(z_1, m_1, z_2, m_2, z_{other}, m_{other})$

$= [f_p(m_1 z_1 + m_2 z_2 + z_{other}) - f_p(m_2 z_1 + m_1 z_2 + z_{other})]S$

$= \frac{S}{k} [I(m_1 z_1) + I(m_2 z_2) + I(z_{other}) - I(m_2 z_1) - I(m_1 z_2) - I(z_{other})]$

$= \frac{S}{k} [\int_{m_2}^{m_1} \frac{\partial I(m z_1)}{\partial m} dm + \int_{m_1}^{m_2} \frac{\partial I(m z_2)}{\partial m} dm] = \frac{S}{k} \int_{m_2}^{m_1} [\frac{\partial I(m z_1)}{\partial m} - \frac{\partial I(m z_2)}{\partial m}] dm < 0$

$\therefore L'(m, z) < L(m, z)$, contradicting with the minimum value of L . Proposition **Q** is True.

Therefore, Proposition **P** is True.

4.Experiments

4.1.Dataset

CUB200-2011[11] is a bird dataset for fine-grained classification testing, where each image has a bird of a specific class. There are a total of 11788 bird images, including 200 different categories of birds. The training set has 5994 images and the test set has 5794 images for the study of classification and segmentation tasks. We randomly select 5 images from each of the 200 classes in the test set to form 1000 images. These 1000 images are tested separately. Comparing the MDM method proposed in this paper with the previous methods[1, 3, 5, 6] on the search effect of classification basis.

NIH-Chest-X-Ray[10] is a publicly available NIH chest X-ray dataset consisting of 112,120 forward-facing X-rays with a total of 14 disease labels, collected from 30,805 independent patients. The image data is divided into 8 training sets and 2 test sets. Among them, there are 880 pictures in the test set with 984 bounding boxes, which frame the corresponding disease positions in the pictures. We use ProtoPNet and XProtoNet trained by the training method in [13] as the pre-trained neural network, and compare the prototype search method of the original paper and the introduction of our proposed MDM in the network. Prototype search effect in the same neural network. Observe the coincidence of the searched activation area and the marked bounding boxes, and compare the accuracy of the two methods on the task of finding prototypes.

Cat and Dog classification dataset. By setting the pre-trained neural network to predict the same image as a cat and a dog, we test whether the MDM can find the correct decision-making regions for classification for different neural networks. Apply the MDM method to neural networks of different architectures [16, 17, 18, 19, 20] and visualize the activation regions it finds as validation. Comparing different neural networks, when predicting different classification results, whether MDM can correctly find the decision area corresponding to the category.

4.2.Evaluation

We choose the activation area performance evaluation indicators as Average Drop and Average Increase proposed by [3]; Deletion and Insertion proposed by [7]. The above four evaluation indicators are widely used for CAM performance comparison. Dice Coefficient, IOU, PPV, Sensitivity of activation area and segmented foreground or detection area. The above eight evaluation indicators are compared.

Average Drop is expressed as $\sum_{i=1}^N \frac{\max(0, Y_i^c - O_i^c)}{Y_i^c}$, and Average Increase is expressed as $\sum_{i=1}^N \frac{\text{Sign}(Y_i^c < O_i^c)}{N}$, where Y_i^c represents the predicted score of class c in the original image i , and O_i^c represents the predicted score of the class c with the explained map obtained after the original image is masked. Sign represents an indicator function that returns 1 if the input is true. Remove certain percentile pixels of the original image to generate a saliency map O_i , which is an evaluation index for comparing Y_i^c and O_i^c predicting scores.

The Deletion and Insertion metrics are complementary to Average Drop and Average Increase. The deletion metric is to remove the predicted activation size of the pixels in the graph according to the saliency map search method from large to small, and then generate the area under the probability curve depicted by the predicted probability result of the picture after removal. If the curve is a sharp drop, the smaller the area below is, it means that the selected pixels are in descending order of importance to the prediction of the neural network, which has a good explanation. On the other hand, the insertion metric is gradually introduced according to the pixel activation size from large to small, and a higher AUC of the area under the probability curve indicates better interpretability of the method.

We believe that when a neural network predicts correctly, it should have large activations for regions that are effective for classification predictions, and low activations for regions that are ineffective for classification predictions. Therefore, we use the Dice Coefficient, IOU, PPV, and Sensitivity of the binary mask generated by the CAM corresponding to the correctly classified neural network under a certain percentile on the foreground image that is conducive to classification as the evaluation indicators. For prototype search of interpretable neural networks [12, 13], we only use these four categories of evaluation metrics to evaluate performance.

4.3.Experimental Details

All mask vectors of MDM are initialized to $\lambda=0.5$ per element. For images of size 224×224 for the CUB dataset and 512×512 for the NIH dataset. We set the $D\{d_i\}_{i=1}^{27}: d_i \in R^{a_i \times b_i \times 1}, a_i = b_i = 5+i, 1 \leq i \leq 27$. Set the threshold $\gamma=5$ for mask conversion to $\{0,1\}$ binary mask. In the CUB dataset, set $\lambda_1=1e-2, \lambda_2=1$. In NIH dataset, set $\lambda_1=1e-3, \lambda_2=1$. Using the Adam optimizer, the learning rate of the update mask is $lr=3e-3$. The activation percentile is set to 90 for all CAMs in the CUB dataset. The CAM activation percentile of ProtoPNet in the NIH dataset is set to 90, and the CAM activation percentile of XProtoNet is set to 80. Each mask is trained separately, and the iteration number is 2000 iterations. The selected network is the network trained on the corresponding dataset after pre-trained on ImageNet.

In CUB200-2011 dataset, using the settings in [12], the number of prototypes for each bird is set to 10, and one prototype is arbitrarily selected from the 10 prototypes as the activation of the network search. Select the first archetype out of 10 archetypes as the activation archetype. In NIH-Chest X-ray dataset, using the settings in [13], the number of prototypes corresponding to each pathology category is set to 3. Since the subsequent detection task is to search for a single pathology, we choose 3 prototypes in Dice. The best performing prototype on Coefficient is used as the activation prototype. By activating the mask feature vector corresponding to the prototype, the activation map can be calculated, and then the area that the neural network pays attention to when making a decision can be known.

4.4.Comparison with Baselines

In the CUB200-2011 bird classification dataset, ResNet and DenseNet are used as pre-trained networks, respectively. MDM and Grad-CAM[1], Grad-CAM++[3], Score-CAM[5], Ablation-CAM[6] these several current state-of-the-art activation map methods are tested, and the performance is compared on the above-mentioned multiple evaluation indicators. The networks used in the comparison of all the different methods below are all networks with the same structure and parameters. We test and compare the performance of different methods when the network parameters are exactly the same.

Table 1. Shows the four evaluation indicators Dice Coefficient, IOU, PPV, Sensitivity results of the four evaluation indicators Dice Coefficient, IOU, PPV, Sensitivity of the neural network ResNet and DenseNet's classification interpretability based on the activation map.

Model	Resnet				Densenet			
	Dice Coefficient	IOU	PPV	Sensitivity	Dice Coefficient	IOU	PPV	Sensitivity
grad-cam	0.261	0.164	0.402	0.217	0.237	0.150	0.370	0.190
grad-cam++	0.434	0.292	0.630	0.365	0.386	0.261	0.560	0.326
score-cam	0.371	0.248	0.557	0.305	0.336	0.222	0.508	0.274
ablation-cam	0.189	0.117	0.285	0.156	0.176	0.112	0.267	0.144
mdm(ours)	0.464	0.323	0.667	0.394	0.421	0.285	0.613	0.353

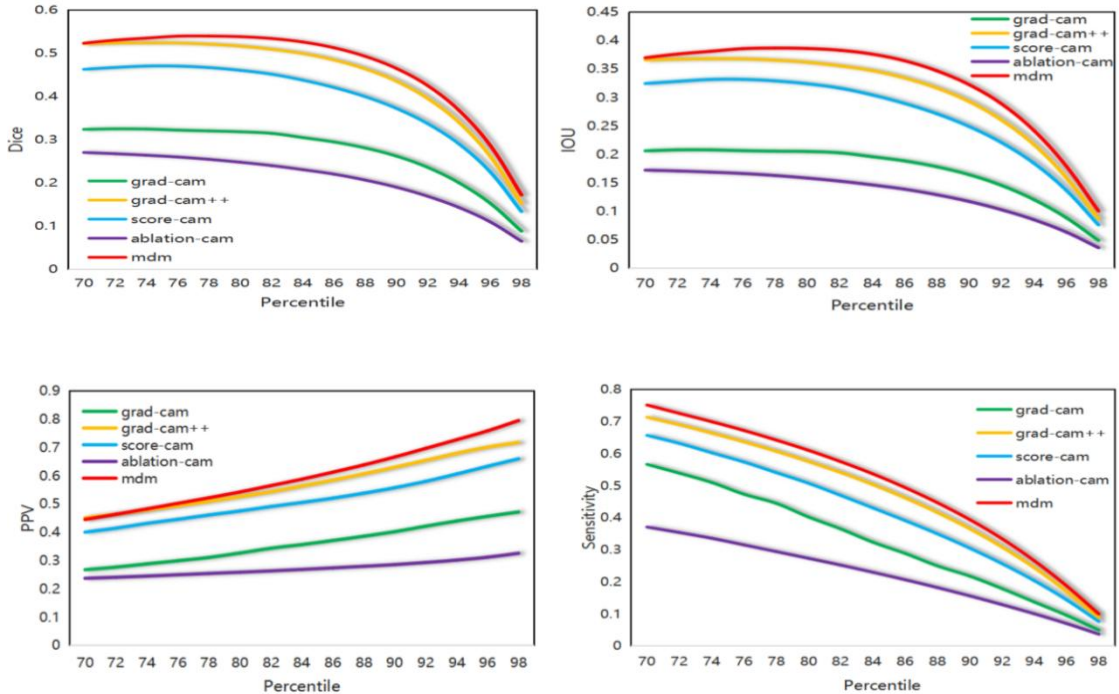


Figure 5. The five models correspond to the probability curves on the four evaluation indicators of Dice Coefficient, IOU, PPV, and Sensitivity when the importance percentile of the masked image pixels is masked from 70 to 99.

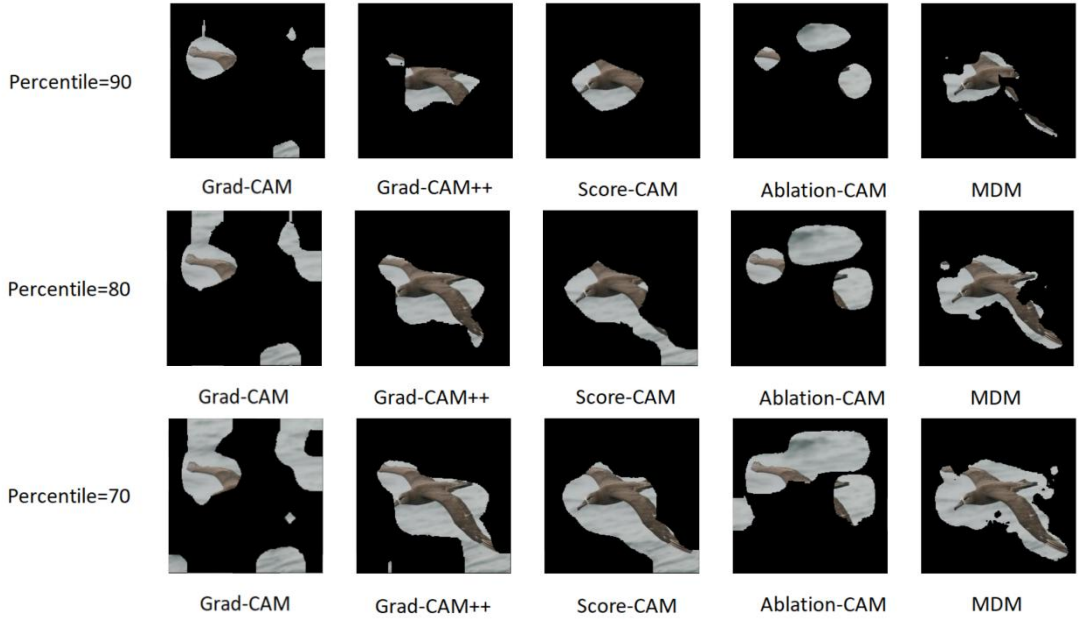


Figure 6. Visualization of the regions concerned by the neural network to make classification decisions when the importance percentages of masked pixels in the binary mask map under different methods are 90, 80, and 70, respectively.

Table 2. Evaluation results on Recognition(lower is better in Average Drop, higher is better in Average Increase).

Method	Grad-CAM	Grad-CAM++	Score-CAM	Ablation-CAM	MDM(ours)
Average Drop(%)	95.82	92.85	91.18	96.69	88.82
Average Increase(%)	0.43	0.85	1.71	0.42	2.14

Table 3. Comparative evaluation in terms of deletion(lower is better) and insertion (higher is better) scores.

Method	Grad-CAM	Grad-CAM++	Score-CAM	Ablation-CAM	MDM(ours)
Deletion	0.134	0.078	0.088	0.286	0.051
Insertion	0.339	0.359	0.391	0.312	0.432

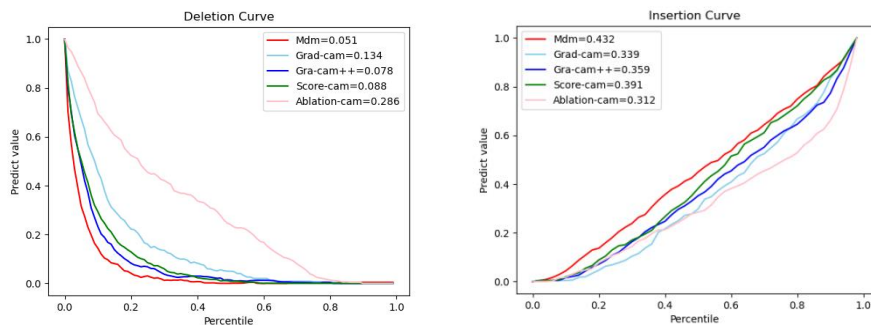


Figure 7. Grad-CAM, Grad-CAM++, Score-CAM, Ablation-CAM and MDM generate saliency maps for representative images with deletion and insertion curves. In deletion curve, faster decline of the curve indicates better performance and smaller AUC , while in increase curve, the faster the curve rises, the better the performance and the greater the AUC.

Table 4. In the CUB-200-2011 bird classification dataset, test the performance comparison of the prototype search effect of ProtoPNet using the original method and the prototype search effect of ProtoPNet using the MDM method on four evaluation indicators.

Dataset Evaluation	CUB200-2011			
	Dice Coefficient	IOU	PPV	Sensitivity
ProtoPNet	0.432	0.287	0.645	0.359
ProtoPNet-mdm(ours)	0.516	0.366	0.738	0.442

Table 5. In NIH dataset, ProtoPNet uses the original method and after using the MDM , the performance comparison of prototype search on four evaluation indicators.

Dataset Evaluation	NIH Chest X-ray			
	Dice Coefficient	IOU	PPV	Sensitivity
ProtoPNet	0.256	0.158	0.263	0.428
ProtoPNet-mdm(ours)	0.283	0.187	0.278	0.486

Table 6. In NIH dataset, XProtoNet compares the performance of prototype search on four evaluation indicators after using the original method and using the MDM.

Dataset Evaluation	NIH Chest X-ray			
	Dice Coefficient	IOU	PPV	Sensitivity
XProtoNet	0.120	0.068	0.070	0.915
XProtoNet -mdm(ours)	0.125	0.071	0.099	0.347

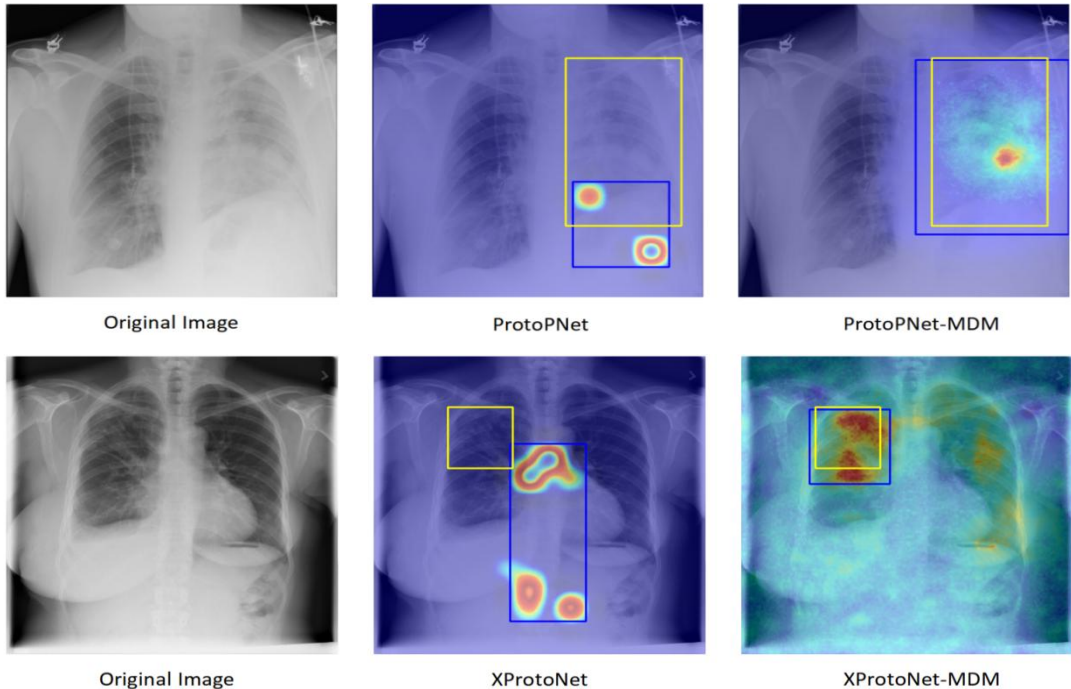


Figure 8. Comparison of the results of ProtoPNet and XProtoNet before and after using MDM. The yellow box represents the real lesion area, and the blue box represents the lesion area found by this method. The activation heatmap area represents the area that the neural network pays most attention to when classifying the condition, i.e. the lesion area. It can be seen from the figure that after using MDM, both ProtoPNet and XProtoNet can find the lesion area better than the original prototype search method.

4.5.Visualization

We mix the activation heatmap generated by MDM with the original image as a visual output. We visualized interpretability predictions for various types of neural networks, convolutional neural networks pre-trained on ImageNet: ResNet50, VGG19, DenseNet121, and Transformer-structured VIT-base (VIT-B) and Swin-Transformer-base(Swin-B), respectively. Observe if the same image is used as input and the neural network is set to predict different categories, whether the region concerned by the activation of the image by the MDM can be used as the basis for decision-making of classification.

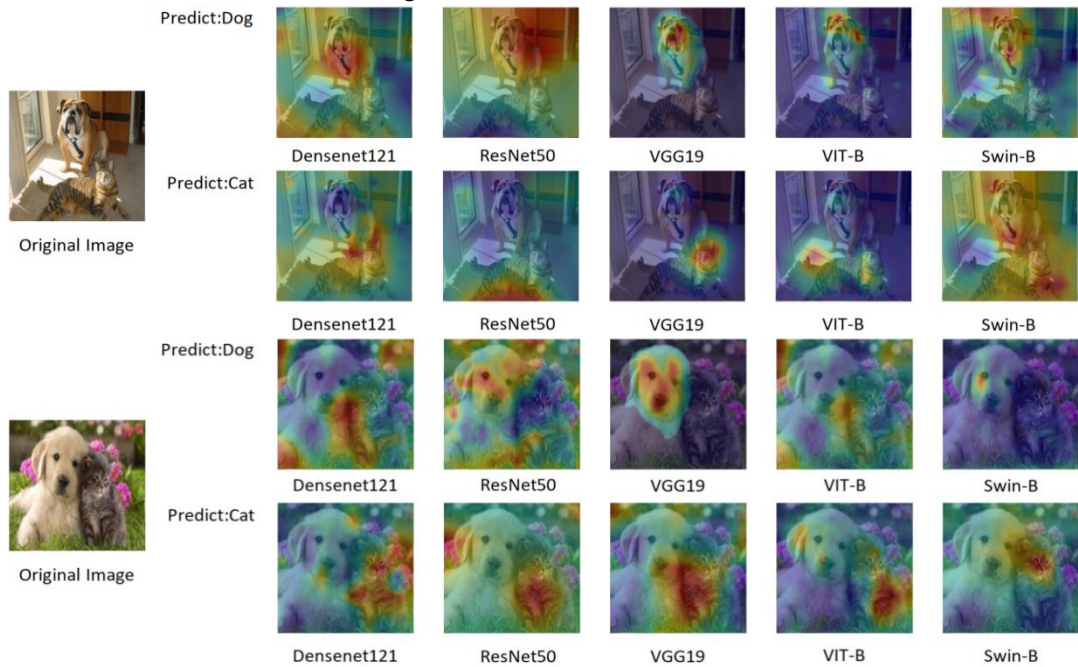


Figure 9. When the predictions are cats and dogs, the MDM calculates a visualization of the areas of interest when making various neural network decisions, from red to blue to indicate the degree of attention from high to low.

Algorithm 1 Mutiple Dynamic Mask processing

Input: Image X_0 , Neural Network f , Activation Position p , Train Epochs C , Learning Rate η , Loss Function L , Loss Weight λ_1, λ_2 , Mask Vector $D\{d_i\}_{i=1}^N$, Threshold γ , Mask Threshold α, β

%stage 1: train mask vector $D\{d_i\}_{i=1}^N$

Initialization;

//get neural network activation a

$A^p \leftarrow f_p(X_0)$

for $i = 1$ to N **do**

for $j = 1$ to C **do**

$M_i \leftarrow \text{Upsample}(d_i)$

 normalize the Mask M_i

$A_i^p \leftarrow f_p(M_i \circ X_0)$

$L_c \leftarrow L(A^p, A_i^p)$

$L_d \leftarrow ||d_i||_1$

$L_t \leftarrow \lambda_1 L_c + \lambda_2 L_d$

$\theta_{d_i} \leftarrow \theta_{d_i} - \eta \frac{\partial L_t}{\partial \theta_{d_i}}$

end for

end for

#stage 2: generate heatmap M^h and binary mask M^b

Initialize M^F : initial zero mask

for $i = 1$ to N **do**

$M_i \leftarrow \text{Upsample}(d_i)$

 normalize the Mask M_i

$M^F = M^F + M_i$

end for

$M^b = \{M^F \geq \gamma\}$

$M^h = M^b \circ M^F$

normalize the Mask M^h

Output: $M_{MDM}^a = \alpha X_0 + \beta M^h$, $M_{MDM}^b = M^b \circ X_0$, M^h , M^b

5. Disuccsion

Note in Table 1, ResNet and DenseNet are used for experiments respectively. On the same deep learning model, compared with the most advanced CAM models in recent years: Grad-CAM, Grad-CAM++, Score-CAM, Ablation-CAM, MDM has greater performance in classification based on activation map foreground search. The performance advantage of MDM's CAM achieves SOTA on interpretable activation based foreground lookup. Figure 5 illustrates: when the occlusion pixel index increases from 70% all the way to 99%, the MDM method has the best foreground finding effect. This shows that MDM has the best performance in explaining the neural network classification foreground finding task. It can be seen from Figure 6 that compared with other methods, the activation map found by MDM retains the activation area at each percentage, which is the most effective area for classification.

Table 2 and Table 3 and Figure 7 show the recently widely used neural network CAM performance evaluation indicators. After each model is masked, it will cause a certain reduction in prediction performance. When we do 90% masking, the remaining data retained by the MDM has the greatest probability of being predicted by the neural network. This shows that MDM is

better than other methods to find out the area that the neural network pays attention to when classifying. According to the insertion and deletion curves, for the masking percentage adjusted from 99% to 1%, the Deletion curve has the smallest AUC on MDM, and the Insertion curve has the largest AUC on MDM. MDM has the steepest curve on both curves than the other methods. This shows that when the most important pixel points in the picture are continuously added and deleted, the pixel point area concerned by MDM is the most favorable point for the neural network to classify in the pixel point area found by other methods. This shows that the performance of MDM for neural network classification decision basis search achieve state-of-the-art.

According to Table 4, for the interpretable network ProtoPNet, after using MDM, the prototype search performance can also be greatly improved. On the traditional bird dataset, after using the MDM method to find the prototype, the network ProtoPNet based on ResNet as the feature extraction backbone, the four evaluation indicators of Dice Coefficient, IOU, PPV, Sensitivity increased by 19.3%, 27.1%, 10.4%, respectively. 22.9%. MDM can greatly improve the search performance of interpretable neural network classification decision basis prototypes.

In medical dataset NIH-Chest X Ray, experiments are carried out on the XProtoNet network and ProtoPNet network with ResNet as the skeleton. Observing the experiments on the four evaluation indicators on 8 pathological prototype searches, it can be seen that when MDM is adopted, ProtoPNet improves the four evaluation indicators of Dice Coefficient, IOU, PPV, and Sensitivity for the prototype search of pathological regions that explain the classification basis. 10.2%, 18.3%, 5.8%, 13.5%. And XProtoNet also has a certain increase in Dice Coefficient, IOU, PPV indicators, and the original XProtoNet method pays attention to too many useless areas, resulting in excessive Sensitivity, and it can be more accurate after using MDM Pay close attention to the lesion area. Due to the limited classification performance of the interpretable neural network for medical images, the performance increase of prototype search after adopting MDM is lower than that of traditional images. According to Figure 8, MDM can better improve the performance of the interpretable neural network in finding the lesion area. The above experiments show that MDM can also be applied to prototype search in clinical medical interpretability classification models. It can better find the lesion area for the diagnosis of pathological categories, make the deep learning model more trusted by clinicians, and promote the application of deep learning models in clinical medical diagnosis.

In Figure 9. The visualization experiment shows that because MDM only uses the input and output of the model, it can be easily adjusted to any neural network. Through visualization experiments, we observed that MDM can not only effectively use classical convolutional neural networks such as ResNet, VGG, and DenseNet, but also VIT and Swin-Transformer on the Transformer architecture. In the activation map, the activation intensity is from red to blue, indicating that the activation intensity is from high to low. When the activation predicted by the control neural network is the result of cat and dog, MDM can well find out the decision when the model makes a classification. The corresponding activation map is generated, and the objects it focuses on are the segmentation foregrounds that are conducive to the classification of the target category. Compared with the 5 models, the VGG network with only convolution operation is the best for CAM search, and other neural networks pay more or less attention to some global information. From this experiment, we can see that the MDM model also has a certain generality, and it can be easily used in neural networks of any structure.

6. Conclusion

Our proposed Mutiple Dynamic Mask can point out important activation regions for neural network classification, and it represents an interpretable basis for neural network classification decisions. The reasoning process of MDM conforms to human cognition and is interpretable. The MDM method is based on learning, it can adaptively find important activation regions for classification, and the performance of MDM in neural network classification decision regions reaches state-of-the-art. MDM can be well used in interpretable neural networks. The prototype search performance of this type of network is improved in the network. The operation process of

MDM only depends on input and output, and it can be applied to most of the most advanced neural networks today. MDM is universal.

7.Reference

[1]R.R.Selvaraju, M.Cogswell, A.Das, R.Vedantam, D.Parikh and D.Batra, “Grad-CAM: Visual Explanations from Deep Networks via Gradient-based Localization, ” in *Proceedings of the IEEE International Conference on Computer Vision*, 2017, pp.618-626.

[2]B.Zhou , A.Khosla , A.Lapedriza , A.Oliva and A.Torralba , “ Learning Deep Features for Discriminative Localization , ” in *Proceedings of the IEEE Conference on Computer Vision and Pattern Recognition*, 2016, pp.2921-2929.

[3]A.Chattopadhyay, A.Sarkar, P.Howlader, V.Balasubramanian, “Grad-CAM++: Generalized Gradient-based Visual Explanations for Deep Convolutional Networks, ” in *Proceedings of the IEEE Winter Conference on Applications of Computer Vision*, 2018, pp.839-847.

[4]Min Lin , Qiang Chen , Shuicheng Yan , “ Network In Network , ” in *Proceedings of the International Conference on Learning Representations*, 2014.

[5]H.Wang , Z.Wang and P.Mardziel , “ Score-CAM:Score-Weighted Visual Explanations for Convolutional Neural Networks, ” in *Proceedings of the IEEE Conference on Computer Vision and Pattern Recognition*, 2020, pp.111-119.

[6]S.Desai and H.G.Ramaswamy, “ Ablation-CAM: Visual Explanations for Deep Convolutional Network via Gradient-free Localization , ” in *Proceedings of the IEEE Winter Conference on Applications of Computer Vision*, 2020, pp.972-980.

[7]V. Petsiuk , A. Das and K. Saenko , “ Rise: Randomized input sampling for explanation of black-box models, ” arXiv preprint arXiv:1806.07421, 2018.

[8]A.Shrikumar, P.Greenside and A.Kundaje, “Learning Important Features Through Propagating Activation Differences, ” in *Proceedings of the International Conference on Machine Learning*, 2017, pp. 3145-3153.

[9]M.Sundararajan , A.Taly and Q.Yan , “ Axiomatic Attribution for Deep Networks , ” in *Proceedings of the International Conference on Machine Learning*, 2017, pp. 3319-3328.

[10]X.Wang, Y.Peng, L.Lu, Z.Lu, M.Bagheri, and R.M.Summers, “Chestx-ray8: Hospital-scale chest x-ray database and benchmarks on weakly-supervised classification and localization of common thorax diseases, ” in *Proceedings of the IEEE Conference on Computer Vision and Pattern Recognition*, 2017, pp. 2097-2106.

[11]C. Wah, S. Branson, P. Welinder, P. Perona, and S. Belongie. The Caltech-UCSD Birds-200-2011 Dataset. Technical Report CNS-TR-2011-001, 2011, California Institute of Technology.

[12]C.Chen, O.Li, C.Tao, AJ.Barnett and J.Su ,C.Rudin, “This Looks Like That: Deep Learning for Interpretable Image Recognition, ” *Advances in Neural Information Processing Systems*, 2019, pp.8930-8941.

[13]E.Kim, S.Kim, M.Seo and S.Yoon, “XProtoNet: Diagnosis in Chest Radiography with Global and Local Explanations, ” in *Proceedings of the IEEE Conference on Computer Vision and Pattern Recognition*, 2021, pp. 15714-15723.

[14]G.Singh and K.Yow, “An Interpretable Deep Learning Model For Covid-19 Detection With Chest X-ray Images, ” in *Proceedings of the IEEE Access*, 2021, pp.85198–85208.

[15]G.Singh and K.Yow, “These do not look like Those: An interpretable deep learning model for image recognition, ” in *Proceedings of the IEEE Access*, 2021, pp.2169-3536.

[16]G. Huang, Z. Liu, L. van der Maaten and K. Q. Weinberger, “Densely Connected Convolutional Networks, ” in *Proceedings of the IEEE Conference on Computer Vision and Pattern Recognition*, 2017, pp.4700–4708.

[17]K. He, X. Zhang, S. Ren, and J. Sun, “Deep Residual Learning for Image Recognition, ” in *Proceedings of the IEEE Conference on Computer Vision and Pattern Recognition*, 2016 , pp.770–778.

[18]K. Simonyan and A. Zisserman, “Very Deep Convolutional Networks for Large-Scale Image Recognition, ” in *Proceedings of the International Conference on Learning Representations*, 2015.

[19]A.Dosovitskiy, L.Beyer, A.Kolesnikov, D.Weissenborn, X.Zhai, T.Underthiner, M.Dehghani, M.Minderer, G.Heigold, S.Gelly, J.Uszkoreit and N.Houlsby, “An image is worth 16x16 words: Transformers for image recognition at scale , ” in *International Conference on Learning Representations*, 2021.

[20]Z.Liu, Y.Lin, Y.Cao, H.Hu, Y.Wei, Z.Zhang, S.Lin and B.Guo, “Swin Transformer: Hierarchical Vision Transformer using Shifted Windows , ” in *Proceedings of the IEEE/CVF International Conference on Computer Vision*, 2021, pp.9992-10002.

[21]C.Patrício, J.C. Neves and L.F. Teixeira, “Explainable Deep Learning Methods in Medical Imaging Diagnosis: A Survey, ” arXiv preprint arXiv:2205.04766, 2022.

[22]J.Deng, W.Dong, R.Socher, L.Li, K.Li and L.Fei-Fei, “ImageNet: A Large-Scale Hierarchical Image Database , ” in *Proceedings of the IEEE Conference on Computer Vision and Pattern Recognition*, 2009, pp.248-255.

[23]Z.Liu, H.Mao, C.Wu, C.Feichtenhofer, T.Darrell,S.Xie, “A ConvNet for the 2020s, ” arXiv preprint arXiv: 2201.03545v2, 2022.

[24]C.Szegedy, W.Liu, Y.Jia, P.Sermanet, S.Reed, D.Anguelov, D.Erhan, V.Vanhoucke, A.Rabinovich, “Going deeper with convolutions, ” in *Proceedings of the IEEE Conference on Computer Vision and Pattern Recognition*, 2015, pp.1-9.

[25] N.Hashimoto, D.Fukushima, R.Koga, Y.Takagi, K.Ko, K.Kohno, M.Nakaguro, S.Nakamura, H.Hontani, I.Takeuchi, “Multi-scale Domain-adversarial Multiple-instance CNN for Cancer Subtype Classification with Unannotated Histopathological Images, ” in *Proceedings of the IEEE Conference on Computer Vision and Pattern Recognition*, 2020, pp.3851-3860.

[26]S.Maksoud, K.Zhao, P.Hobson, A.Jennings, B.C. Lovell, “SOS: Selective Objective Switch for Rapid Immunofluorescence Whole Slide Image Classification, ” in *Proceedings of the IEEE Conference on Computer Vision and Pattern Recognition*, 2020, pp.3861-3870.